Core–shell microstructures in $0.68Pb(Fe_{2/3}W_{1/3})O_3$–$0.32PbTiO_3$ at the morphotropic phase boundary

2005 J. Phys.: Condens. Matter 17 2167

(http://iopscience.iop.org/0953-8984/17/13/014)

INSTITUTE OF PHYSICS PUBLISHING JOURNAL OF PHYSICS: CONDENSED MATTER

J. Phys.: Condens. Matter **17** (2005) 2167–2175 doi:10.1088/0953-8984/17/13/014

Core–shell microstructures in $0.68Pb(Fe_{2/3}W_{1/3})O_3$–$0.32PbTiO_3$ at the morphotropic phase boundary

Zhenrong Li[1,3], Aiying Wu[1], P M Vilarinho[1,4] and Ian M Reaney[2]

[1] Department of Ceramics and Glass Engineering, CICECO, University of Aveiro, 3810-193 Aveiro, Portugal
[2] Department of Engineering Materials, University of Sheffield, Sheffield Sl 3JD, UK

Received 19 December 2004, in final form 16 February 2005
Published 18 March 2005
Online at stacks.iop.org/JPhysCM/17/2167

Abstract

The domain structures of ceramics with the morphotropic phase boundary (MPB) composition 0.68PFW–0.32PT were analysed *in situ* by TEM as a function of temperature from 16 to 300 K. A core–shell structure was detected at room temperature, in which the core of the grains was Ti rich and the shell W rich with respect to the bulk composition. At 16 K, a macrodomain state is observed throughout the volume of the grains, but at >250 K a domain-free shell is formed around a central core that still exhibits strong domain wall strain contrast in two-beam conditions. The presence of the core–shell microstructure and the growth of the core on cooling is correlated with the appearance of (*h*00)/(00*l*) peak splitting in XRD traces as temperature decreases and is used to interpret the dielectric data.

1. Introduction

$Pb(Fe_{2/3}W_{1/3})O_3$ (PFW) is a relaxor ferroelectric that exhibits a diffuse and frequency dependent dielectric permittivity maximum at low temperature (∼185 K). Similar to other complex Pb based perovskite relaxors, the macroscopic properties of PFW can be tailored by the formation of multicomponent systems, e.g., $(1-x)Pb(Fe_{2/3}W_{1/3})O_3$–$xPbTiO_3$ (PFW–PT). Recently, there has been renewed interest in studying this system due to possible multiferroic and magnetoelectric properties [1, 2]. Previous studies [3–6] on the PFW–PT system have shown that, as the PT content increases, the temperature of the dielectric maximum increases and the relaxor ferroelectric behaviour gradually becomes a normal ferroelectric. A maximum in the dielectric permittivity was observed for compositions in the range of $0.20 < x < 0.37$. X-ray diffraction (XRD), infrared and Raman spectroscopy have revealed that samples with

[3] Present address: Electronic Materials Research Laboratory, Key Laboratory of Education Ministry, Xi'an Jiaotong University, Xi'an 710049, People's Republic of China.
[4] Author to whom any correspondence should be addressed.

$0.20 < x < 0.37$ lie within or close to a morphotropic phase boundary (MPB), in which pseudocubic and tetragonal phases coexist [3, 4]. The MPB in the PFW–PT system is temperature and field dependent. At room temperature (300 K) the MPB exists between $0.30 \leqslant x \leqslant 0.35$ [7], but despite the interesting physical properties of PFW–PT MPB compositions, there has been very little attention paid to its domain structure.

Transmission electron microscopy (TEM) is an effective method of evaluating the domain structure of ferroelectric materials. Weak beam and two-beam dark field imaging techniques can elucidate the domain wall distributions and their associated strain fields whilst imaging with superlattice reflections can illustrate the complex domain structures associated with cell-doubling phase transitions such as ordering [8] or octahedral tilting [9]. Notably, in relaxor-based systems, the domain structures of $(1 - x)Pb(Mg_{1/3}Nb_{2/3})O_3$–$xPbTiO_3$, (PMN–PT) ceramics were analysed by Viehland *et al* [10]. Micron-sized ferroelectric domains were observed for $x > 0.40$ but tweedlike structures were found for the MPB composition, $x = 0.35$. TEM studies by Baba-Kishi *et al* [11] on PMN–PT, $x = 0.33$ single crystals showed that two kinds of domain configurations existed: lamellae of 90° domains typical of the tetragonal phase and irregular sets of domains associated with the rhombohedral phase [11].

In the related $Pb(Ni_{1/3}Nb_{2/3})O_3$–$PbZrO_3$–$PbTiO_3$ (PNN–PZ–PT) system, herringbone domain structures were observed for compositions near the MPB [12]. In contrast, $Pb_{0.85}La_{0.1}(Zr_{0.53}Ti_{0.47})O_3$ (close to the MPB) exhibited a combination of micron-, nano- and tweedlike-domain structures at room temperature, demonstrating that normal and disordered ferroelectric states coexist for this system [13]. To date, most TEM studies of relaxor–ferroelectric materials have been performed at room temperature. For PFW–PT, work has concentrated on dielectric and structural characterization [3–7, 14] but no TEM studies of the domain structure have been reported. Moreover, the observed dependence of the MPB of the PFW–PT system on the temperature requires evaluation of the domain structure also as a function of the temperature. In this paper, the domain structure of the MPB composition, 0.68PFW–0.32PT, is studied by *in situ* TEM between 16 and 300 K. The data are correlated with the temperature dependence of the structure and dielectric properties.

2. Experimental procedures

0.68PFW–0.32PT ceramics were prepared by a conventional mixed oxide method using reagent-grade PbO, WO_3, Fe_2O_3, and TiO_2 (Merck) raw materials. The preparation procedure of the ceramics has been previously described [14], but in brief samples were sintered at 950 °C for 3 h in a sealed alumina crucible. To compensate for the PbO loss, a PbO-rich atmosphere was maintained during the sintering by placing an equimolar mixture of PbO and ZrO_2 inside the crucible.

The phase structure of the sintered samples was analysed by XRD (Philips X'pert MPD, equipped with a Rantoom-Baar chamber) from 80 to 380 K in order to elucidate changes in structure. Specifically, diffraction peaks around 45° were slow scanned (0.03 °C min^{-1}) to accurately determine the presence and extent of splitting of the (200)/(002) reflections associated with tetragonal symmetry. For dielectric property measurements, gold electrodes were sputtered on both sides of the samples and data collected using an HP4284A impedance analyser in conjunction with a cryostat and furnace for low and high temperature experiments, respectively. Data were collected at 10 kHz, 100 kHz, and 1 MHz to assess the frequency dependence of any peaks in permittivity and loss. Samples for TEM were first ground flat and mechanically thinned to 25 μm. A 3 mm diameter copper ring with a 2 mm diameter hole was then glued onto the thinned ceramics. Samples were further ion thinned using a RES100 ion mill, operated at accelerating voltage of 3 kV, a beam current of 1.4 mA per gun, and

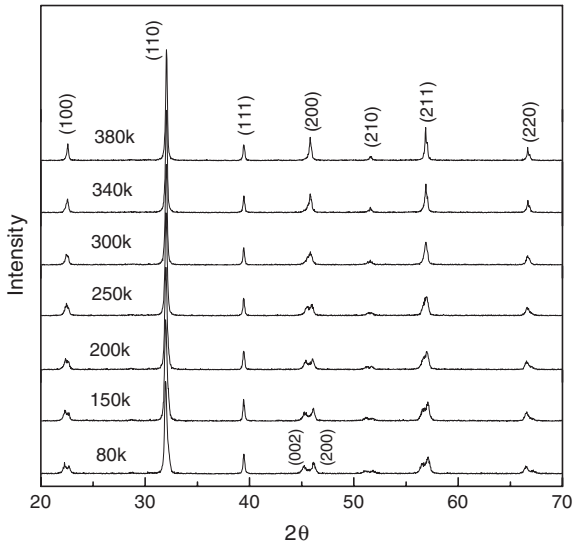

Figure 1. Temperature dependence of XRD curves for 0.68PFW–0.32PT ceramics.

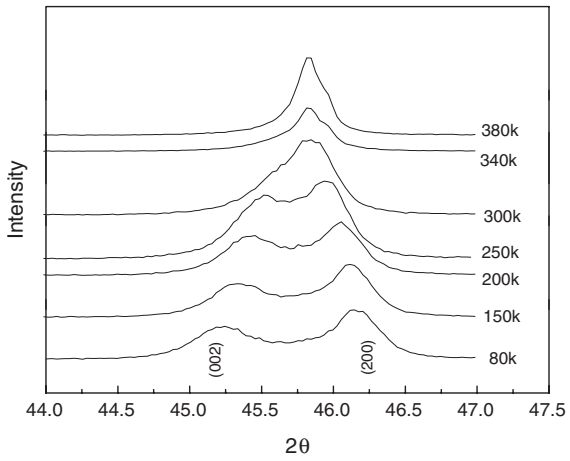

Figure 2. Temperature dependence of (002)/(200) peaks for 0.68PFW–0.32PT ceramics.

with incidence angles of $\sim 10^{\circ}$. The samples were examined using Hitachi H9000-NA TEM operated at 300 kV. Samples were cooled *in situ* from 16 to 300 K using a Hitachi H9000-NA liquid helium cold stage. Semi-quantitative chemical analysis was performed using energy-dispersive x-ray spectroscopy (EDS, Roentec).

3. Results

Figure 1 shows the XRD patterns for 0.68PFW–0.32PT ceramics from 80 to 380 K. The sample is monophasic within the limits of XRD and with the perovskite structure, with $a \approx 3.963$. At $\geqslant$340 K the sample exhibits cubic symmetry, whereas at $\leqslant$250 K splitting of the (220), (211), (210), (200) and (100) peaks is observed, indicating tetragonal symmetry. Figure 2 illustrates

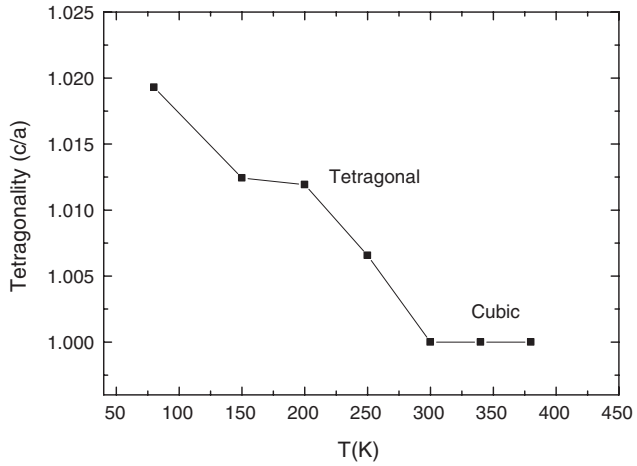

Figure 3. Temperature dependence of tetragonality c/a ratio for 0.68PFW–0.32PT ceramics.

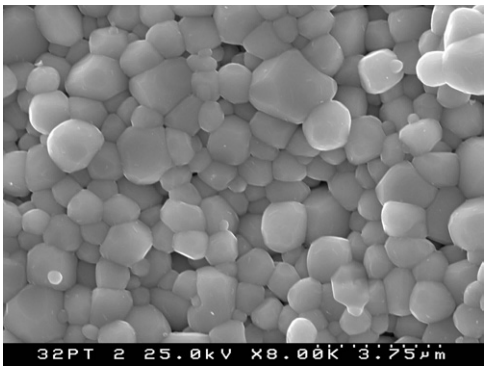

Figure 4. Secondary electron SEM image of 0.68PFW–0.32PT ceramics.

in more detail the splitting of the (200) reflection as a function of temperature and figure 3 shows the temperature dependence of the c/a ratio. The exact onset of the phase transition from cubic to tetragonal is difficult to determine but at 300 K the (200) peak is asymmetric (figure 2), suggesting that it occurs either at or above this temperature at least in some regions of the sample. SEM analysis at room temperature (figure 4) revealed a dense microstructure with an average grain size of 1–2 μm. No other remarkable features were observed.

The evolution of domain structure in 0.68PFW–0.32PT ceramics with increasing temperature was studied by *in situ* TEM. Figures 5(a) and (b) are TEM bright-field images at 16 and 300 K, respectively. At 16 K, all perovskite grains exhibited a lamellar domain structure throughout their volume, as illustrated in figure 5(a). As temperature increased to $>$250 K, a faint core–shell microstructure is formed. The core–shell microstructure further developed in which the central region still contained strain contrast from the domain walls whereas the exterior or shell of the grains were free from domain wall contrast, as shown in figure 5(b) (300 K, room temperature). Figure 6 shows EDS traces from (a) the core of a grain exhibiting the domain structure at room temperature and (b) the shell, free from domain wall contrast. Each trace contains Pb, Ti, W, and Fe consistent with the batched oxides. Cu is present since, as discussed in the experimental section, a Cu support ring is used in sample

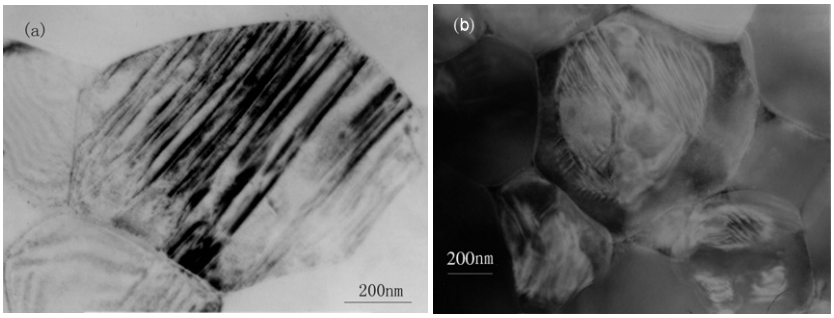

Figure 5. Bright-field TEM images for 0.68PFW–0.32PT obtained at different temperatures: (a) 16 K and (b) 300 K (room temperature).

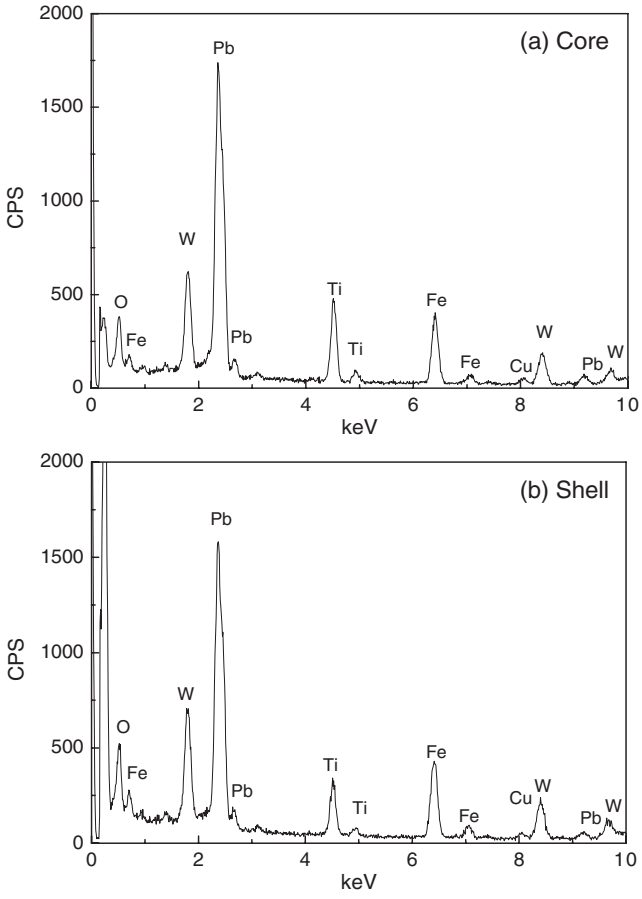

Figure 6. EDS analysis of core and shell in figure 5(b).

preparation. However, the core region of each grain is Ti rich and W deficient with respect to the shell. These observations are consistent in all core–shell regions and enrichment of the Ti concentration was observed for all regions which exhibited a domain structure at room temperature. At triple junctions and along some grain boundaries, TEM revealed the presence of an amorphous phase which was rich in PbO and WO_3, as analysed by EDS. The position

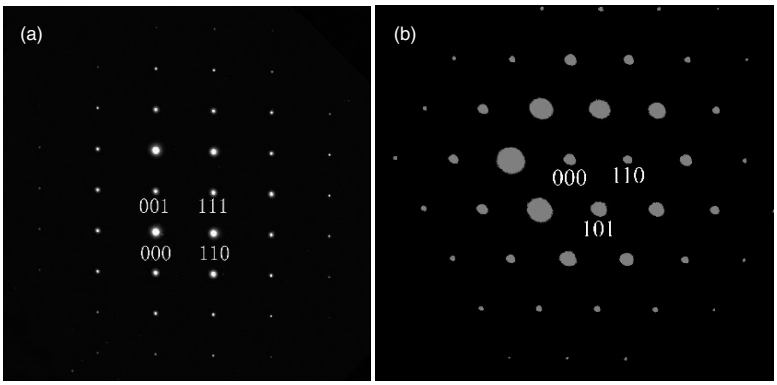

Figure 7. ⟨110⟩ (a) and ⟨111⟩ (b) zone axis of selected-area electron diffraction (SAED) pattern of 0.68PFW–0.32PT at room temperature.

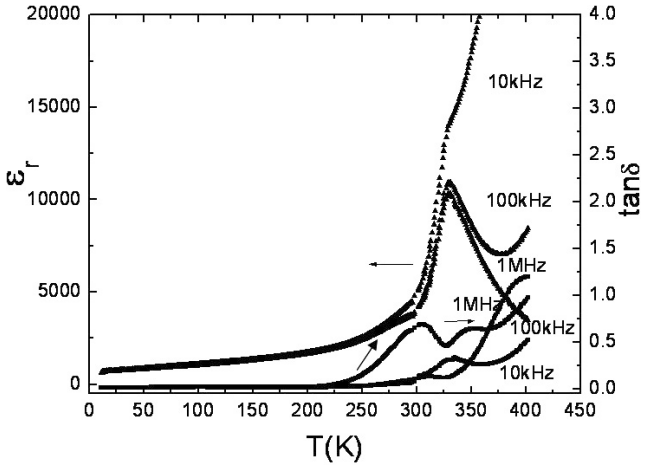

Figure 8. Temperature dependence of dielectric properties for 0.68PFW–0.32PT ceramics.

of the amorphous phase within the microstructure suggests that it was originally liquid at the sintering temperature but solidified on cooling. PbO–WO_3 forms a eutectic at 730 °C [15] so it is likely that the liquid phase acts as a sintering aid during densification.

Figures 7(a) and (b) are ⟨110⟩ and ⟨111⟩ selected-area electron diffraction (SAED) patterns from grains of 0.68PFW–0.32PT obtained at room temperature. No superlattice reflections are observed and the diffraction data from the core and shell regions were identical. Electron diffraction patterns were unaffected by cooling and there was no evidence of further phase transitions other than the formation of domains in the grain shells.

The temperature dependence of the dielectric permittivity and loss for 0.68PFW–0.32PT are shown in figure 8. As frequency increases from 10 kHz to 1 MHz, the contribution to the total permittivity due to the displacement of space charge decreases and a maximum of the dielectric permittivity, presumably corresponding to the cubic–tetragonal phase transition, is observed at ∼330 K. At 1 MHz, the peak in permittivity decreases in magnitude but does not increase in temperature, suggesting that the material is a normal but lossy ferroelectric rather than relaxor. Above 330 K, the dielectric permittivity at 10 KHz and dielectric losses at all

frequencies increase with increasing temperature, probably due to an increase in conductivity which is related to electron holes, as previously reported [14].

XRD traces indicated that the onset temperature of the cubic–tetragonal transition occurs between 300 and 340 K (figure 2), consistent with the dielectric data. In addition, the room temperature TEM images reveal that the core regions of many grains have undergone a structural phase transition. The XRD, TEM and dielectric data are therefore self-consistent and indicate that the majority of the sample transforms from cubic to tetragonal at ∼330 K but that the outer shells of many grains transform only on further cooling. By 16 K, all the material has completely transformed to the tetragonal phase and the c/a ratio increases.

4. Discussion

Core–shell microstructures are typically observed in modified X7R $BaTiO_3$ (BT) based ceramics [16–18] where the shell is heterogeneously doped, giving rise to a distribution of T_cs, and the core is undoped. The shells are typically doped with oxides such as ZrO_2, Nb_2O_5, and Ce_2O_3, whose role is to stabilize the temperature dependence of the permittivity of $BaTiO_3$ ceramics to within ±15% of the room temperature value, e.g., for X7R materials. The formation of a core–shell structure in BT ceramics is achieved by the addition of dopants and is therefore not an intrinsic feature of the system.

The results presented in this work demonstrate that at room temperature the MPB composition of the PFW–PT system, 0.68PFW–0.32PT, exhibits a core–shell microstructure. In the core of the grains a well defined domain structure is clearly observed at room temperature but the shell is featureless, only transforming to tetragonal and forming a domain structure on cooling.

EDS analyses (figure 6(a) for the core and (b) for the shell) revealed that as with $BaTiO_3$ the core–shell microstructure and its subsequent temperature dependence (figure 5) is related to compositional heterogeneity. However, unlike $BaTiO_3$, it is postulated that the heterogeneity is an intrinsic feature of the PFW–PT system. It is well known that liquid phase sintering mechanism(s) is/are thought to be present during the sintering of PbO-based ceramic perovskites because of the low melting point of PbO (888 °C). In the PbO–WO_3 binary phase diagram, the lowest eutectic temperature is 730 °C [15], below the sintering temperature of PFW–PT ceramics (950 °C). It is therefore proposed that in the early stages of the sintering process a WO_3 rich liquid phase is formed which acts as a sintering aid. After the initial shrinkage and densification, W ions diffuse inward from the grain boundary phase towards the grain core and the Fe and Ti ions diffuse outward. However, the diffusion of W/Fe/Ti ions through the perovskite grains is via the solid state and is therefore slow with respect to the initial densification. The net result is that the outer regions (shells) of the grains on average are rich and their centres (cores) deficient in W. The formation of the core–shell structure is therefore related to chemical micro-inhomogeneity arising from the relatively slow solid state diffusion of W/Fe/Ti ions. One consequence of this mechanism is that the formation of the core–shell microstructure and therefore chemical homogeneity should be strongly dependent on heat treatment schedule. The true MPB is considered to be the composition at which a homogenous distribution of constituent ions is able to sustain the coexistence of two phases of similar free energy. A heterogeneous distribution of constituent ions, even intragranular as discussed above, would result in an MPB range rather than specific composition and this may well explain the breadth of the MPB previously reported by the authors [3, 4]. This aspect of the PFW–PT system will be the subject of further study.

Several reports of core–shell structures in lead-based complex relaxor ferroelectrics have been published. In the $Pb(Mg_{1/3}Nb_{2/3})O_3$–$PbTiO_3$–$Pb(Mg_{1/2}W_{1/2})O_3$ sys-

tem with excess WO_3, the core was identified as rich in the PMN–PT solid solution and the shell rich in PMW [19]. Similar results were observed in the $Pb(Mg_{1/2}W_{1/2})O_3$–$PbTiO_3$–$Pb(Ni_{1/3}Nb_{2/3})O_3$ system with WO_3 excess [20]. According to these authors, the formation of the core–shell microstructure was probably related to the use of excess WO_3. However, in $0.1Pb(Mg_{1/2}W_{1/2})O_3$–$0.3Pb(Ni_{1/3}Nb_{2/3})O_3$–$0.6PbTiO_3$ (PMW/PNN/PT, 10/30/60) a core–shell microstructure formed without the addition of excess WO_3, but as the PMW concentration increased the core–shell microstructure was no longer observed [21]. Such observations are in contrast to Yang *et al* [22] who reported an Fe-rich core, W-rich shell microstructure in undoped $Pb(Fe_{2/3}W_{1/3})O_3$ ceramics, as observed in the present work for the PFW–PT system. Despite the diversity of the reported data on WO_3 based perovskites, it is evident that the presence of a W-rich shell is consistent in all studies and all authors agree that there is a liquid phase sintering mechanism involving a PbO–WO_3 eutectic phase. From this perspective, the mechanism of core–shell formation in 0.68PFW–0.32PT proposed in this study is plausible.

Although the precise recorded temperatures of *in situ* TEM studies are open to debate due to electron beam heating of the sample during observation, the core–shell microstructure became a prominent feature at >250 K. According to XRD, the c/a ratio suddenly decreases (figure 3) on heating around this temperature and only a slight asymmetry of the (200) is observed at 300 K (figure 2). From TEM observations, at >250 K, the core region shrinks on heating, implying that the shell is undergoing a gradual ferroelectric–paraelectric phase transition over a broad temperature interval. There is small increase in the gradient ($\Delta\varepsilon_r/\Delta T$) of the permittivity data at ∼250 K (arrowed), prior to the onset of the large dielectric anomaly at 330 K (figure 8) which may arise from the broad ferroelectric to paraelectric phase transition in the shell regions, but this requires further confirmation.

5. Conclusions

The microstructural evolution of 0.68PFW–0.32PT ceramics was studied from 16 to 300 K using *in situ* TEM. At 16 K all grains exhibited a macrodomain structure throughout their volume, but at ∼250 K the outer regions of the grain became featureless whilst the grain interiors retained strain contrast due to the presence of domain walls. EDS analysis revealed that the cores were Ti and the shells W rich with respect to the batched composition. A liquid phase (PbO–WO_3 eutectic) sintering mechanism is proposed to explain the formation of the core–shell microstructure in the PFW–PT system.

Acknowledgment

The first author would like to thank CICECO (http://www.ii.ua.pt/ciceco), University of Aveiro, Portugal, for financial support.

References

[1] Mitoseriu L, Marre D, Siri A S and Nanni P 2003 Magnetic properties of $Pb(Fe_{2/3}W_{1/3})O_3$–$PbTiO_3$ solid solutions *Appl. Phys. Lett.* **83** 5509–11

[2] Ivanov S A, Eriksson S-G, Tellgren R and Rundlof H 2004 Neutron powder diffraction study of the magnetoelectronic relaxor $Pb(Fe_{2/3}W_{1/3})O_3$ *Mater. Res. Bull.* **39** 2317–28

[3] Mitoseriu L, Vilarinho P M and Baptista J L 2002 Phase coexistence in $Pb(Fe_{2/3}W_{1/3})O_3$–$PbTiO_3$ solid solutions *Appl. Phys. Lett.* **80** 4422–4

[4] Vilarinho P M, Zhou L, Mitoseriu L, Finocchio E, Soares M R and Baptista J L 2002 Morphotropic phase boundary in $Pb(Fe_{2/3}W_{1/3})O_3$–$PbTiO_3$ system *Ferroelectrics* **270** 253–8

[5] Feng L and Ye Z-G 2002 Phase diagram and phase transitions in the relaxor ferroelectric $Pb(Fe_{2/3}W_{1/3})O_3$–$PbTiO_3$ system *J. Solid State Chem.* **163** 484–90
[6] Mitoseriu L, Stancu A, Fedor C and Vilarinho P M 2003 Analysis of the composition-induced transition from relaxor to ferroelectric state in $Pb(Fe_{2/3}W_{1/3})O_3$–$PbTiO_3$ solid solutions *J. Appl. Phys.* **94** 1918–25
[7] Mitoseriu L, Vilarinho P M, Viviani M and Baptista J L 2003 Structural studies of $Pb(Fe_{2/3}W_{1/3})O_3$–$PbTiO_3$ system *Mater. Lett.* **57** 609–14
[8] Randall C A, Barber D J and Whatmore R W 1987 *In situ* TEM experiments on perovskite-structured ferroelectric relaxor materials *J. Microscopy* **145** 275–91
[9] Zheng H, Reaney I M, Lee W E, Jones N and Thomas H 2002 Effects of octahedral tilting on the piezoelectric properties of strontium/barium/niobium-doped soft lead zirconate titanate ceramics *J. Am. Ceram. Soc.* **85** 2337–44
[10] Viehland D, Kim M-C, Xu Z and Li J-F 1995 Long-time present tweedlike precursors and paraelectric clusters in ferroelectric containing strong quenched randomness *Appl. Phys. Lett.* **67** 2471–3
[11] Baba-Kishi K Z, Pang G K H, Choy C L, Chan H L W, Luo H S, Yin Q R and Yin Z W 2001 Transmission electron microscopy study of the domain structure of the relaxor ferroelectric PMN–PT 67/33 single crystal *Ferroelectrics* **253** 55–62
[12] Zhu X H, Zhu J M, Zhou S H, Li Q, Meng Z Y, Liu Z G and Ming N B 2000 Domain morphology evolution associated with the relaxor–normal ferroelectric transition in the Bi- and Zn-modified $Pb(Ni_{1/3}Nb_{2/3})O_3$–$PbZrO_3$–$PbTiO_3$ system *J. Eur. Ceram. Soc.* **20** 1251–5
[13] Gupta S M, Li J-F and Viehland D 1998 Coexistence of relaxor and normal ferroelectric phases in morphotropic phase boundary compositions of lanthanum-modified lead zirconate titanate *J. Am. Ceram. Soc.* **81** 557–64
[14] Vilarinho P M, Zhou L, Manfred Pockl L, Marques N and Baptista J L 2000 Dielectric properties of $Pb(Fe_{2/3}W_{1/3})O_3$–$PbTiO_3$ solid-solution ceramics *J. Am. Ceram. Soc.* **83** 1149–52
[15] *Phase Diagrams for Ceramists* 1975 Supplement 1975 (Columbus, OH: The American Ceramic Society)
[16] Hennings D and Rosenstein G 1984 Temperature-stable dielectrics based on chemically inhomogeneous $BaTiO_3$ *J. Am. Ceram. Soc.* **67** 249–54
[17] Park Y and Kim H-G 1997 Dielectric temperature characteristics of cerium-modified barium titanate based ceramics with core–shell grain structure *J. Am. Ceram. Soc.* **80** 106–12
[18] Yoon S-H, Lee J-H and Kim D-Y 2002 Core–shell structure of acceptor, coarse barium titanate grains *J. Am. Ceram. Soc.* **85** 3111–3
[19] Uchikoba F and Sawamura K 1993 Core–shell domain structure in lead complex perovskite materials *Japan. J. Appl. Phys.* **32** 4258–60
[20] Uchikoba F, Ito T and Nakajima S 1995 X7R lead-complex perovskite dielectrics with inhomogeneous compositional distribution *Japan. J. Appl. Phys.* **34** 2374–9
[21] Furuya M, Mori T and Ochi A 1994 Transmission electron microscopy study of B-site cation configurations in perovskite-structured $Pb(Mg_{1/2}W_{1/2})O_3$–$Pb(Ni_{1/3}Nb_{2/3})O_3$–$PbTiO_3$ ceramics *J. Appl. Phys.* **75** 4144–51
[22] Yang R-Y, Lin M-H and Lu H-Y 2001 Core–shell structure in pressureless-sintered undoped $Pb(Fe_{2/3}W_{1/3})O_3$ ceramics *Acta Mater.* **49** 2597–607